Characterization of the interaction of multivalent glycosylated ligands with bacterial lectins by biolayer interferometry

Léo Picault, Eugénie Laigre, Emilie Gillon, Claire Tiertant, Olivier Renaudet, Anne Imberty, David Goyard, Jerome Dejeu

Characterization of the interaction of multivalent glycosylated ligands with bacterial lectins by BioLayer Interferometry

L. Picault[1], E. Laigre[1], E. Gillon[2], C. Tiertant[1], O. Renaudet[1], A. Imberty[2], D. Goyard[1*], J. Dejeu[1,3*]

[1] Université Grenoble Alpes, CNRS, DCM, UMR 5250, 570 Rue de la Chimie, 38000 Grenoble, France.

[2] Université Grenoble Alpes, CNRS, CERMAV, UPR5301, 601 Rue de la Chimie, 38000 Grenoble, France

[3] FEMTO-ST Institute, CNRS UMR-6174, Université de Bourgogne Franche-Comté, F-25000 Besançon, France

*To whom correspondence should be addressed: J. Dejeu: Tel: +33-363-082-623; e-mail: Jerome.dejeu@univ-grenoble-alpes.fr; D. Goyard: Tel: +33-456-520-862; e-mail: David.goyard@univ-grenoble-alpes.fr

Keywords: Biolayer Interferometry/Glycoclusters/Glycodendrimers /Lectins/Multivalency

Supplementary Data Included: Figures S1 – S26 and Tables SI – SII

Abstract

The study of multivalent carbohydrate–protein interactions remains highly complicated and sometimes rendered impossible due to aggregation problems. Bio-Layer Interferometry (BLI) is emerging as a tool to monitor such complex interactions. In this study, various glycoclusters and dendrimers were prepared and evaluated as ligands for lectins produced by pathogenic bacteria *Pseudomonas aeruginosa* (LecA and Lec B) and *Burkholderia ambifaria* (BambL). Reliable kinetic and thermodynamic parameters could be measured, and immobilization of either lectin or ligands resulted in high quality data. The methods gave results in full agreement with previous ITC experiments, and presented strong advantages since they require less quantity and purity for the biomolecules.

Introduction

Carbohydrate–lectin interactions play central roles in a number of physiological and pathological processes such as cell adhesion, cancer metastasis or viral and bacterial infections (Sharon 1996; Lis and Sharon 1998; Gabius et al. 2011; Cummings 2019). Taken individually, these interactions are typically weak (low millimolar to high micromolar range) but lectins, given their multimeric structure, capitalize on the high density of carbohydrates present at the cell surface to form high avidity complexes (Lee and Lee 1995; Mammen et al. 1998; Lundquist and Toone 2002). In this context, synthetic multivalent structures such as glycoclusters and glycodendrimers have the ability to compete with cell surface glycans to hamper pathogen adhesion to host cells. Understanding these multivalent interactions is of highest interest but still remains challenging because of the diversity of structural parameters that influence these processes. Biolayer interferometry (BLI) is emerging as a potent tool for the characterization of biomolecular interactions (Concepcion et al. 2009). This optical method enables real-time, label-free analysis of interactions providing information on affinity as well as kinetics using one of the interacting partners in solution in a microwell plate and the second one immobilized at the surface of a biosensor tip. BLI is based on the interferometry change resulting from the optical mass variation upon biomolecular interaction. This optical mass is not only dependent on the refractive index variation (and therefore to the molecular weight of the compound) but also on the sensing layer thickness. Compared to other techniques such as surface plasmon resonance (SPR) and isothermal titration calorimetry (ITC), BLI presents the advantage to be less sensitive to external factors such as aggregation and microfluidic troubles and its use is increasingly widespread in the study of protein-protein (Machen et al. 2018) or DNA-small molecule interactions (Bonnat et al. 2019; Gillard et al. 2019; Vignon et al. 2020). Recently, we have reported the first evaluation of a series of multivalent glycoconjugates towards the hexameric αGalNAc-specific *Helix pomatia* agglutinin (HPA), used as a model lectin immobilized on the BLI sensors as described in Figure 1 (Laigre et al. 2018). The thermodynamic dissociation constants (K_d) determined by BLI were consistent with the enzyme-linked lectin assay (ELLA) (Hoang et al. 2017).

In this paper, this method was extended to three other lectins. LecA and LecB are virulence factors produced by *Pseudomonas aeruginosa*, with specificity for galactose and fucose, respectively (Gilboa-Garber 1982). They are both homotetramers but with different topologies and presentation of their four binding sites (Figure 2) (Mitchell et al. 2002; Cioci et al. 2003). BambL is a fucose-specific lectin from another opportunistic pathogen, *Burkholderia ambifaria,* with trimeric association of tandem repeats resulting in six binding sites on the same face of a donut-shape structure (Figure 2) (Audfray et al. 2012).

The results obtained were compared with previous ITC experiments and demonstrated a good concordance between the two techniques. The originality of this study is to demonstrate the versatility of BLI, by anchoring either the lectins or the multivalent ligands (glycoclusters) on the biosensor. With those three bacterial lectins, it was demonstrated that whatever the immobilized interacting partner, the thermodynamic and kinetics parameters were concordant.

Results

A set of both previously identified (Pifferi et al. 2017; Goyard et al. 2019) and original multivalent ligands displaying either fucose or galactose moieties were synthetized. These glycoclusters and glycodendrimers were built from two different tetravalent scaffolds, a cyclodecapeptide or a polylysine dendron. The latter were prepared by solid-phase peptide synthesis (SPPS) incorporating chemically modified amino acids displaying either azide or aldehyde functions (Bossu et al. 2011; Pifferi et al. 2017). Conjugation with propargyl or aminooxy glycosides were achieved *via* copper-catalyzed azide alkyne cycloaddition (CuAAC) and oxime ligation respectively. The resulting multivalent glycoconjugates are depicted in figure 3 (see ESI for synthetic protocols and new compounds characterizations).

For LecA and LecB, the binding properties of the tetravalent ligands were previously determined by ITC (Goyard et al. 2019). However, in the case of trimeric BambL, aggregation phenomenon during the titration with multivalent fucosylated ligands led to unexploitable data. To circumvent this issue and determine binding parameters, biolayer interferometry (BLI) assays - for which the lectins are

immobilized on a sensor - were performed. This technique was previously used to efficiently characterize the interaction between the *Helix pomatia agglutinin* (HPA) lectin and hexadecavalent GalNAc-functionalized glycoconjugates (Laigre et al. 2018).

Interaction between immobilized LecB and multivalent glycoconjugates

After immobilization of biotinylated LecB on a streptavidin-coated BLI tip, the binding was evaluated with two tetravalent cyclopeptide (R4oFuc **1**, R4tFuc **2**) and two polylysine-based (D4oFuc **3**, D4tFuc **4**) compounds, functionalized with αFuc moieties with either triazole or oxime linkages (Figure 4-A to D).

In all sensorgrams (Figure 4-A to D), the signal increased with the concentration. The plateau was not reached for the lowest concentrations for conjugates **1**-**4** during the association step, but the curvature was sufficient to obtain the overall kinetic parameters of the interaction. In all sensorgrams, a fast association was observed, while the dissociation is much slower, resulting in a shape characteristic of rebinding processes in multivalent interactions. Due to the weak dissociation of our lectin-ligand systems, the data were fitted only for the association step in order to determine k_{obs}.(Sanchez Perez et al. 2021) As the latter depends on both kinetic association rate k_{on} and dissociation rate k_{off} through the following relation $k_{obs} = k_{on}*C + k_{off}$, k_{obs} variations were plotted as a function of the glycoconjugate concentration C (Figure S 17), leading to the determination of both kinetic constants k_{on} and k_{off} and to the calculation of the thermodynamic dissociation constant K_d by using the following relation $K_d=(k_{off}/k_{on})$ (Figure 4-G and Table I).

In agreement with previously obtained ITC data, no significant variations of the K_d values were observed for the four tetravalent glycoconjugates **1**-**4** (blue lines in Figure 4-G and Table 1). The kinetic constants were also similar with k_{on} and k_{off} values about 10^4 $M^{-1}.s^{-1}$ and 10^{-3} s^{-1}, respectively. This result indicates that the nature of the scaffold and the linkage of the fucose moiety on the scaffold does not drastically influence the ligand-LecB interaction. Compared to the K_d values determined by ITC, the ones determined by BLI are lower by a factor of 3-4 for the tetravalent conjugates (100 nM by BLI *versus* 350 nM by ITC), a phenomenon presumably due to the local concentration effect of sugar units provided

by the glycocluster immobilization. Both techniques led to K_d in the same range, with non-significant differences.

To enhance further the affinity, the valency of the glycoconjugates was increased from 4 to 16 following the experimental procedure previously reported by the group of Renaudet (Goyard et al. 2019). Since the nature of the sugar-scaffold linkage does not impact on the binding properties of the tetravalent glycoconjugates with LecB, only the two hexadecavalent analogs RR16tFuc **6** and DD16tFuc **7**, with triazole spacers, were synthetized from a combination of cyclopeptide and/or polylysine scaffolds (Figure 3) and evaluated by BLI (Figure 4-E and F). In contrast with the trend observed for the tetravalent conjugates, the dissociation step was drastically impacted by the nature of the structure of the hexadecavalent conjugate (Figure 4-E and F). Indeed, conjugate RR16tFuc **6** - composed of two layers of cyclopeptide scaffolds and displaying the most rigid structure - led to the highest k_{off} with a value of 2.10^{-3} s^{-1} (Figure 4-G and Table I, obtained from Figure S 18). By comparison, the analog DD16tFuc **7**, which has a more flexible structure, offered a k_{off} of 4.10^{-5} s^{-1}, showing almost no ligand-lectin dissociation. Despite the high k_{off} of **6**, the K_d of the latter was still improved by a factor of 10 - by comparison with the tetravalent analogs - reaching a value of 19 nM, mainly due to a high k_{on} of $1.2.10^5$ $M^{-1}.s^{-1}$ (Figure 4-G and Table I). With an equivalent k_{on}, the conjugate **7** unsurprisingly displayed a lower K_d with a value of 0.3 nM, corresponding to a 100-fold affinity compared to the panel of tetravalent conjugates. Therefore, even if the nature of the structure of the hexadecavalent conjugates **6** and **7** did not have an influence on the association step, it drastically impacted the dissociation step, with a better dissociation observed for the most rigid structure **6**. Regarding the K_d evaluations, the results obtained by BLI are concordant with the previously published studies, reporting for instance a K_d of 44 nM determined by ITC for a similar hexadecavalent conjugate (Goyard et al. 2019). This gain in affinity has been previously rationalized by molecular modelling (Berthet et al. 2013). In the cited study, it has been shown that hexadecavalent fucosylated glycodendrimers built on the same scaffold, can easily accommodate four monomers of LecB without encountering any steric clashes. This result was also in agreement with the stoichiometries observed by ITC. Furthermore, the ball-shape of LecB, presenting four binding sites with different orientations is favourable for cross-linking of multivalent ligands explaining also the high avidity for hexadecavalent conjugates.

Several units of α-mannose, an alternative ligand of LecB that displays a 100 fold weaker affinity than α-fucose (71 µM),(Sabin et al. 2006), were grafted on a tetravalent scaffold to afford the conjugate R4tMan **8**. The binding affinity of the latter was then compared to the monovalent control (Figure S 19). As expected, despite a 7-fold improvement (K_d of 10 µM, Figure 4-G and Table SII), the affinity remained weak due to both low association and high dissociation rates (respectively 6.10^2 $M^{-1}.s^{-1}$ and 6.10^{-3} s^{-1}). No interaction occurred with galactosylated cluster R4tGal **5** as control (Figure S 20), thus confirming the absence of unspecific interaction with the lectin. All these results confirm the higher specificity of LecB for αFuc-functionalized conjugates.

Interaction between immobilized BambL and multivalent glycoconjugates

The αFuc-functionalized glycoconjugates were assessed with BambL immobilized on the sensor. By contrast with LecB which has a tetrameric structure, BambL is a trimeric protein displaying six binding sites for fucose, all located on the same face of the donut like protein fold (Figure 2). For this assay campaign, only compounds with triazole spacers were evaluated, namely R4tFuc **2**, D4tFuc **4**, RR16tFuc **6** and DD16tFuc **7** (Figure 5).

With this lectin, whatever the multivalent glycoconjugates used, the dissociation was slow (Figure 5-E). As above, the association part of the sensorgram was fitted by a 1:1 model to extract the k_{obs} value (Figure S 21) and to determine the kinetic association and dissociation constants for each ligand (Figure 5-E and Table II). The experiments pointed out the impact of the glycoconjugate's structure on the lectin-ligand interaction. Concerning the tetravalent conjugates **2** and **4**, an improvement by a factor of more than 6 was observed depending on the structure. Actually, the rigid structure of **2** led to a K_d of 46 nM when compared to the more flexible structure of **4** with a K_d of 7 nM. Similarly to the experiments conducted with LecB, the k_{on} values were drastically impacted by the nature of the structure with k_{on} from 3.10^4 $M^{-1}.s^{-1}$ for **2** to $1.3.10^5$ $M^{-1}.s^{-1}$ for **4** – that is to say 4 times higher for **4** than for **2**. Concerning the k_{off} values, no important differences were highlighted for the two structures.

Similar interaction trends were observed for the hexadecavalent analogs. No variations of the k_{off} were observed, but the more flexible ligand DD16tFuc **7** led to a higher k_{on} – with a value of $6.3.10^4$ $M^{-1}.s^{-1}$ –

when compared to RR16tFuc **6**, which exhibits a k_{on} of $3.6.10^4$ $M^{-1}.s^{-1}$. As a result, the K_d values of 20 nM for **6** and 10 nM for **7** were directly impacted by difference in association constant.

In conclusion, if the nature of the ligand's structure influenced the interaction with BambL – with a stronger interaction observed with flexible scaffolds – the valency of the ligand did not seem to have a significant impact on the resulting affinity. The most efficient ligands (**4** and **7**) exhibited K_d around 10 nM and affinity gains between 20 to 100 compared to the monovalent control (Audfray et al. 2012), but this represents only a weak improvement when comparing to tetravalent **2** or **4** (Figure 5-E and Table II). In the β-propeller topology of BambL, all sites are close to each other (17 Å, versus 40-48 Å for LecB) and on the same face. As soon as two or three sites are engaged in binding to a multivalent ligand, a strong gain in binding is observed, due to efficient rebinding, as demonstrated with b-propellers with number of sites varied by engineering (Arnaud et al. 2013). Increasing further the valency of the ligands does not result in strong increase of affinity.

The interaction specificity of BambL was confirmed with tetravalent αMan- and βGal-functionalized conjugates used as negative controls (Figure S 22), where no signals were observed.

Interaction between immobilized LecA and multivalent glycoconjugates

We finally studied the interactions between LecA and βGal-functionalized conjugates (R4tGal **5** and RR16tGal **9**) by BLI that were previously evaluated by ITC (Goyard et al. 2019) (Figure 6).

The shape of the sensorgrams depends on the valence of the glycoconjugate. When the valency increases, the kinetic dissociation constant decreases whereas the association one increases. After fitting of the association part and extraction of the k_{obs} (Figure S 23), the tetravalent conjugate R4tGal **5**, the dissociation constant reached a K_d of 750 nM with a k_{on} of $1.2.10^4$ $M^{-1}.s^{-1}$ and a k_{off} of $9.2.10^{-3}$ s^{-1} (Figure 6-C and Table III).

For the hexavalent analog RR16tGal **9**, an affinity in the nanomolar range was obtained, with a K_d of 6 nM, implying a 100-fold improvement compared to tetravalent compound **5** (Figure 6-C). This strong interaction with LecA was explained by a higher association (around $8.0.10^4$ $M^{-1}.s^{-1}$) and a lower dissociation rate ($4.5.10^{-4}$ s^{-1}) than those of **5** (Figure 6-C and Table III). To briefly compare with the

ITC experiments, although the K_d of **5** determined by BLI is slightly higher than the one measured by ITC, it is consistent with other studies previously conducted, describing a several hundred nanomolar-range K_d (Cecioni et al. 2012; Cecioni et al. 2015). Similarly, the K_d of **9** determined by BLI is in the same range of affinity than the one of 14 nM measured by ITC (Goyard et al. 2019).

The specificity of the interaction between LecA and the Gal-functionalized glycoconjugates was confirmed with R4tFuc **2** cluster (Figure S 24) where no signal was measured.

Glycan immobilization

In the above experiments, and in those reported in the literature, the lectin is immobilized on the sensor and the glycosylated ligand is in solution in the 96-wells plate (Figure 1). In the present study, we decided to test a new system and to reverse the experimental format, by immobilizing the ligand on the sensor chip and assaying the lectin in solution (Figure 7). This removes the risk of affecting the lectin functionality by a chemical modification of an amino acid involved in ligand recognition. The experimental design is also closer to the biological situation of soluble lectins binding to glycoconjugates on cell surface. To efficiently compare the results with those described above, only tetravalent glycoclusters were chosen to be evaluated as ligands for LecA, LecB and BambL. Two biotinylated glycoconjugates, R4tFuc-biotin **10** and R4tGal-biotin **11** (Figure 3), functionalized either with αFuc or βGal units, were synthesized and immobilized on streptavidin-coated BLI sensors. The results from these experiments are compiled in Figure 8.

The kinetic dissociation constants depend on the glycocluster immobilized on the BLI sensors while the association one depends on the lectin in solution. Indeed, no dissociation was observed for the R4tFuc-functionalized sensor contrary to R4tGal-functionalized one, while the association constants obtained with BambL and LecA were greater than the one obtained with LecB. The kinetic constants were determined from the k_{obs} values extracted by fitting the association step with a 1:1 model (Figure S 25 and Table IV). Both in terms of kinetics and thermodynamics, the observed results are consistent with k_{on}, k_{off} and K_d values relatively similar for all the ligand-lectin couples, whatever the partner that is grafted on the sensor's surface (Figure 8-D).

The specificity of the ligand-lectin interaction was controlled by cross-testing (Figure S 26). No significant BLI signals were recorded when the Gal-functionalized conjugate was immobilized on the

surface and dipped in LecB or BambL solution at 1 µM. The same observation was made when the Fuc-functionalized conjugate was dipped in the LecA solution at 1 µM.

Materials and Methods

All chemical compounds were purchased from Sigma Aldrich and Novabiochem. Lectins were recombinantly expressed in *E. coli* and purified as previously described (Mitchell et al. 2005; Blanchard et al. 2008; Audfray et al. 2012). Biotinylation was performed as indicated by the provider (reference B3295 Sigma).

Buffer. Lectin solutions were prepared in Buffer 1 (PBS 1X, 0.1 mM $CaCl_2$ pH 7.4) and glycoconjugate solutions were prepared in Buffer 2 (0.1 mM Tris HCl, 0.035 mM $CaCl_2$ pH 7.4).

Bio Layer Interferometry (BLI). BLI sensors coated with streptavidin (SA sensors) were purchased from Forte Bio (PALL). Prior to use, they were immerged for 10 minutes in Buffer 2 to remove the protective sucrose layer from the sensor surface. The sensors were dipped for 15 minutes in Buffer 1 solution containing 100 nM of biotinylated interaction partner (lectin or glycoconjugate depending on the experiment). Afterwards the functionalized sensors were rinsed with Buffer 1 for 10 minutes to remove the unbound molecules. For the association step, the sensors were dipped – for a time span depending on the kinetic constant – in analyte solutions prepared beforehand at different concentrations (see Table SI). Each association step was followed by a dissociation step consisting in rinsing the sensors in Buffer 2 for 300 or 2000 seconds. Another sensor, not functionalized with the lectin, was used as a reference blank sample. The experimental steps have been summarized in Figure 1.

Data analysis

All association steps were fitted using a 1:1 model to determine k_{obs} values (Lecarme et al. 2016; El-Aziz et al. 2017). The k_{obs} parameter depends on both the kinetic association rate k_{on} and dissociation rate k_{off}, with the following relation $k_{obs} = k_{on}*C + k_{off}$, where C is the analyte concentration present in solution. Plotting k_{obs} as a function of C led to the determination of the two kinetic constants with k_{on} as the slope of the curve and k_{off} as the intercept for C=0. The reported values were obtained from the average of independent experiments, and the errors provided are standard deviations relatively to the

mean. Each experiment was repeated at least three times for the multivalent ligands and two times for the reference samples and negative controls.

Conclusion

Using BLI, we were able to measure affinities for tetravalent and hexadecavalent ligands to bacterial lectins, obtaining affinities in the nanomolar range. These results are in good agreement with previously published ITC studies, which confirms the reliability of biolayer interferometry to study multivalent carbohydrate protein interactions. Some differences are observed, for example in the case of LecA, which is expected due to the differences in experimental conditions, with both partners in solution for ITC, and one partner immobilized on a surface for BLI. The topologies of lectins themselves can also influenced the dependence to presentation (surface or solution) or to valency. Lectins with binding sites oriented in different directions (LecB) act as cross-linkers in solution, while the ones with binding sites in same direction (BambL) bind strongly to glycosurfaces.

Besides determining both kinetic and thermodynamic parameters, BLI offers the advantages to be fast, operates at low cost and requires small quantities of both lectin and ligand compared to other analytical techniques such as ITC and SPR. The other advantages compared to the SPR is the possibility to use the solutions deposited in the 96-wells plate for several experiments. Added to that, the regeneration solution used to dissociate the lectin-conjugate complex can also be recovered and subsequently analyzed. Our studies highlighted the possibility to use modified ligands on BLI tips for characterizing the interaction with unlabeled lectins in solution. Indeed, with the use of biotinylated tetravalent conjugates and lectins, the kinetic and thermodynamic constants do not depend on which partner is immobilized on the BLI sensor. In fact, similar results were obtained for lectin or conjugate grafted on the sensor. It should be noted that such observation would not be valid for all lectins, since some of them maybe less active when immobilized. Functionalizing BLI tip with the multivalent ligand could be considered as the safer method, as well as the one that mimics best the presentation of multivalent ligands on cell surfaces. These last results pave the way for the search of new lectins by biolayer interferometry screenings.

Indeed, this new approach could be used to fish new lectins out of complex media before identification by mass spectrometry.

Acknowledgement

This work was supported by CNRS, Université Grenoble Alpes, the French ANR project Glyco@Alps (ANR-15-IDEX-02), Labex ARCANE, and CBH-EUR-GS (ANR-17-EURE-0003). The authors also acknowledge support from ICMG UAR 2607 for BLI facilities. OR acknowledges the European Research Council Consolidator Grant LEGO (647938) for EL, CT and DG.

References

Arnaud J, Claudinon J, Tröndle K, Trovaslet M, Larson G, Thomas A, Varrot A, Römer W, Imberty A, Audfray A. 2013. Reduction of Lectin Valency Drastically Changes Glycolipid Dynamics in Membranes but Not Surface Avidity. *ACS Chem Biol*. 8:1918–1924.

Audfray A, Claudinon J, Abounit S, Ruvoën-Clouet N, Larson G, Smith DF, Wimmerová M, Le Pendu J, Römer W, Varrot A, et al. 2012. Fucose-binding lectin from opportunistic pathogen Burkholderia ambifaria binds to both plant and human oligosaccharidic epitopes. *J Biol Chem*. 287:4335–4347.

Berthet N, Thomas B, Bossu I, Dufour E, Gillon E, Garcia J, Spinelli N, Imberty A, Dumy P, Renaudet O. 2013. High affinity glycodendrimers for the lectin LecB from Pseudomonas aeruginosa. *Bioconjugate Chem*. 24:1598–1611.

Blanchard B, Nurisso A, Hollville E, Tetaud C, Wiels J, Pokorna M, Wimmerova M, Varrot A, Imberty A. 2008. Structural Basis of the Preferential Binding for Globo-Series Glycosphingolipids Displayed by Pseudomonas aeruginosa Lectin I. *J Mol Biol*. 383:837–853.

Bonnat L, Dautriche M, Saidi T, Revol-Cavalier J, Dejeu J, Defrancq E, Lavergne T. 2019. Scaffold stabilization of a G-triplex and study of its interactions with G-quadruplex targeting ligands. *Org Biomol Chem*. 17:8726–8736.

Bossu I, Šulc M, Křenek K, Dufour E, Garcia J, Berthet N, Dumy P, Křen V, Renaudet O. 2011. Dendri-RAFTs: a second generation of cyclopeptide-based glycoclusters. *Org Biomol Chem*. 9:1948–1959.

Cecioni S, Imberty A, Vidal S. 2015. Glycomimetics versus multivalent glycoconjugates for the design of high affinity lectin ligands. *Chem Rev*. 115:525–561.

Cecioni S, Praly JP, Matthews SE, Wimmerová M, Imberty A, Vidal S. 2012. Rational design and synthesis of optimized glycoclusters for multivalent lectin-carbohydrate interactions: Influence of the linker arm. *Chem Eur J*. 18:6250–6263.

Cioci G, Mitchell EP, Gautier C, Wimmerová M, Sudakevitz D, Pérez S, Gilboa-Garber N, Imberty A. 2003. Structural basis of calcium and galactose recognition by the lectin PA-IL of Pseudomonas aeruginosa. *FEBS Lett*. 555:297–301.

Concepcion J, Witte K, Wartchow C, Choo S, Yao D, Persson H, Wei J, Li P, Heidecker B, Ma W, et al. 2009. Label-free detection of biomolecular interactions using BioLayer interferometry for kinetic characterization. *Comb Chem High Throughput Screening*. 12:791–800.

Cummings RD. 2019. "Stuck on sugars – how carbohydrates regulate cell adhesion, recognition, and signaling." *Glycoconjugate J*. 36:241–257.

El-Aziz TMA, Ravelet C, Molgo J, Fiore E, Pale S, Amar M, Al-Khoury S, Dejeu J, Fadl M, Ronjat M, et al. 2017. Efficient functional neutralization of lethal peptide toxins in vivo by oligonucleotides. *Sci Rep*. 7:7202.

Gabius HJ, André S, Jiménez-Barbero J, Romero A, Solís D. 2011. From lectin structure to functional glycomics: Principles of the sugar code. *Trends Biochem Sci*. 36:298–313.

Gilboa-Garber N. 1982. Pseudomonas aeruginosa lectins. *Methods Enzymol*. 83:378–385.

Gillard M, Laramée-Milette B, Deraedt Q, Hanan GS, Loiseau F, Dejeu J, Defrancq E, Elias B, Marcélis L. 2019. Photodetection of DNA mismatches by dissymmetric Ru(ii) acridine based complexes. *Inorg Chem Front*. 6:2260–2270.

Goyard D, Thomas B, Gillon E, Imberty A, Renaudet O. 2019. Heteroglycoclusters With Dual Nanomolar Affinities for the Lectins LecA and LecB From Pseudomonas aeruginosa. *Front Chem*. 7:666.

Hoang A, Laigre E, Goyard D, Defrancq E, Vinet F, Dumy P, Renaudet O. 2017. An oxime-based glycocluster microarray. *Org Biomol Chem*. 15:5135–5139.

Laigre E, Goyard D, Tiertant C, Dejeu J, Renaudet O. 2018. The study of multivalent carbohydrate-

protein interactions by bio-layer interferometry. *Org Biomol Chem*. 16:8899–8903.

Lecarme L, Prado E, De Rache A, Nicolau-Travers M-L, Gellon G, Dejeu J, Lavergne T, Jamet H, Gomez D, Mergny J-L, et al. 2016. Efficient Inhibition of Telomerase by Nickel-Salophen Complexes. *ChemMedChem*. 11:1133–1136.

Lee YC, Lee RT. 1995. Carbohydrate-Protein Interactions: Basis of Glycobiology. *Acc Chem Res*. 28:321–327.

Lis H, Sharon N. 1998. Lectins: Carbohydrate-Specific Proteins That Mediate Cellular Recognition. *Chem Rev*. 98:637–674.

Lundquist JJ, Toone EJ. 2002. The Cluster Glycoside Effect. *Chem Rev*. 102:555–578.

Machen AJ, O'Neil PT, Pentelute BL, Villar MT, Artigues A, Fisher MT. 2018. Analyzing Dynamic Protein Complexes Assembled On and Released From Biolayer Interferometry Biosensor Using Mass Spectrometry and Electron Microscopy. *J Vis Exp*. 138:e57902.

Mammen M, Choi S-K, Whitesides GM. 1998. Polyvalent interactions in biological systems: implications for design and use of multivalent ligands and inhibitors. *Angew Chem Int Ed*. 37:2755–2794.

Mitchell E, Houles C, Sudakevitz D, Wimmerova M, Gautier C, Pérez S, Wu AM, Gilboa-Garber N, Imberty A. 2002. Structural basis for oligosaccharide-mediated adhesion of Pseudomonas aeruginosa in the lungs of cystic fibrosis patients. *Nat Struct Biol*. 9:918–921.

Mitchell EP, Sabin C, Šnajdrová L, Pokorná M, Perret S, Gautier C, Hofr C, Gilboa-Garber N, Koča J, Wimmerová M, et al. 2005. High affinity fucose binding of Pseudomonas aeruginosa lectin PA-IIL: 1.0 Å resolution crystal structure of the complex combined with thermodynamics and computational chemistry approaches. *Proteins: Struct Funct Genet*. 58:735–746.

Pifferi C, Goyard D, Gillon E, Imberty A, Renaudet O. 2017. Synthesis of Mannosylated Glycodendrimers and Evaluation against BC2L-A Lectin from Burkholderia Cenocepacia. *Chempluschem*. 82:390–398.

Sabin C, Mitchell EP, Pokorná M, Gautier C, Utille JP, Wimmerová M, Imberty A. 2006. Binding of different monosaccharides by lectin PA-IIL from Pseudomonas aeruginosa: Thermodynamics data correlated with X-ray structures. *FEBS Lett*. 580:982–987.

Sanchez Perez E, Toor R, Bruyat P, Cepeda C, Degardin M, Dejeu J, Boturyn D, Coche-Guérente L. 2021. Impact of Multimeric Ferrocene-containing Cyclodecapeptide Scaffold on Host-Guest Interactions at a β-Cyclodextrin Covered Surface. *ChemPhysChem*. 22:2231–2239.

Sharon N. 1996. Carbohydrate—Lectin Interactions in Infectious Disease. In: Kahane I, Ofek I, editors. Toward Anti-Adhesion Therapy for Microbial Diseases. Springer US. (Advances in Experimental Medicine and Biology). p. 1–8.

Vignon A, Flaget A, Michelas M, Djeghdir M, Defrancq E, Coche-Guerente L, Spinelli N, Van der Heyden A, Dejeu J. 2020. Direct Detection of Low-Molecular-Weight Compounds in 2D and 3D Aptasensors by Biolayer Interferometry. *ACS Sensors*. 5:2326–2330.

Legends to figures

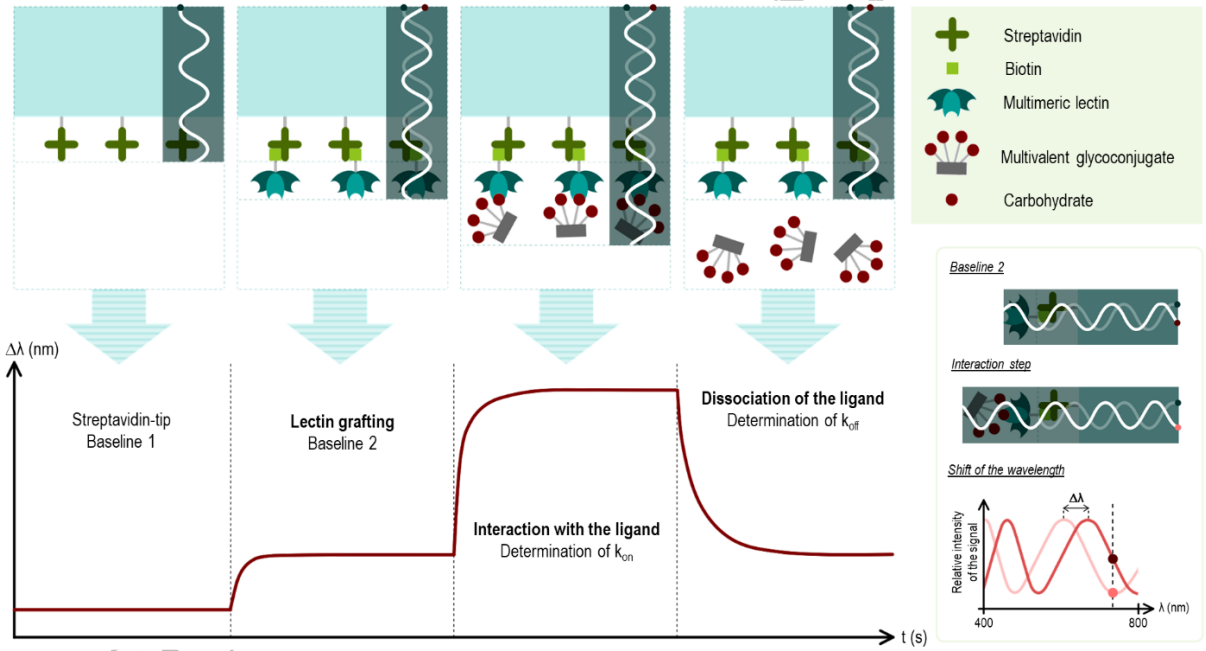

Figure 1: Schematic representation of the design used for evaluation of the interaction between multimeric lectins and multivalent ligands by biolayer interferometry (BLI)

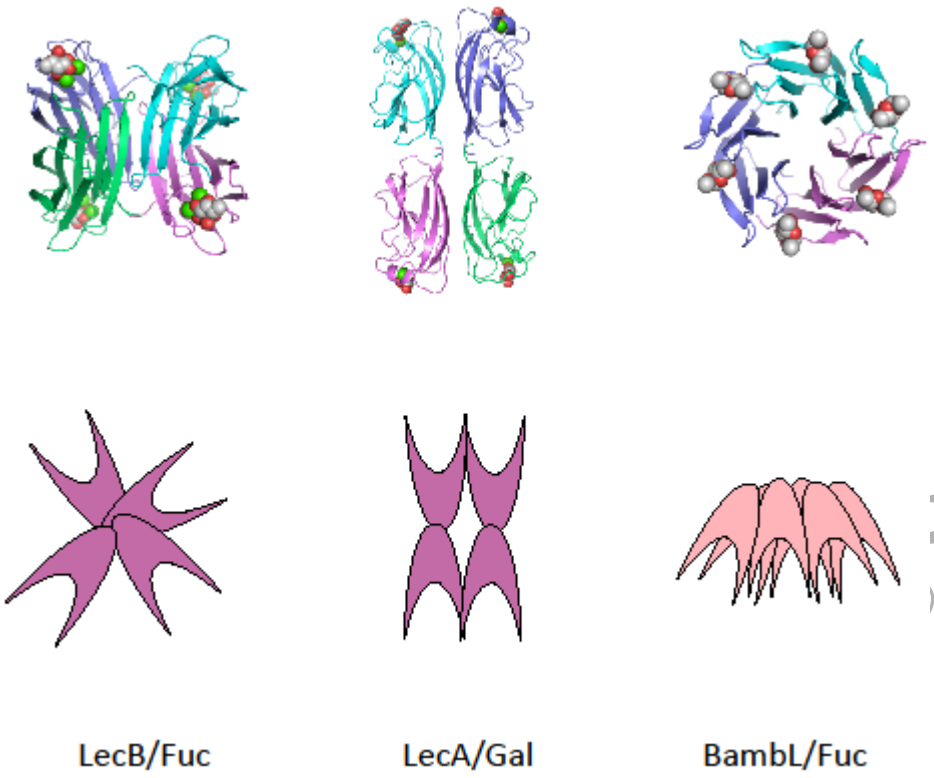

Figure 2: Structures (top) and schematic representation (bottom) of the lectins used in this study, LecB (PDB 1GZT), LecA (PDB 1OKO) and BambL (adapted from PDB 3ZZV). Proteins are represented as ribbons, sugars and ions as spheres (Pymol).

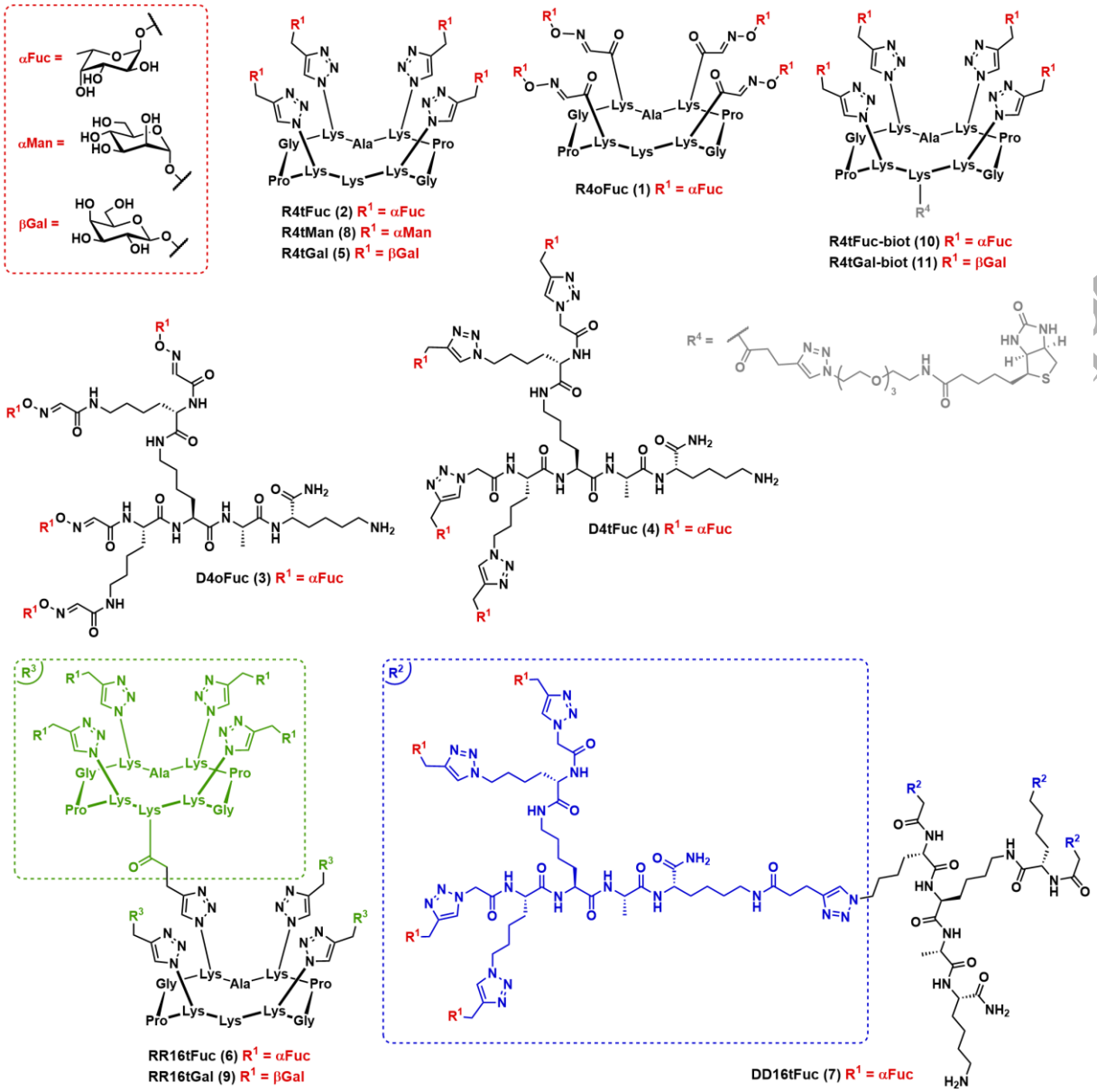

Figure 3: Structures of previously identified (**1**, **2**, **5**, **6**, **8**, **9**) and new (**3**, **4**, **7**, **10**, **11**) multivalent glycoconjugates evaluated as lectin ligands by BLI.

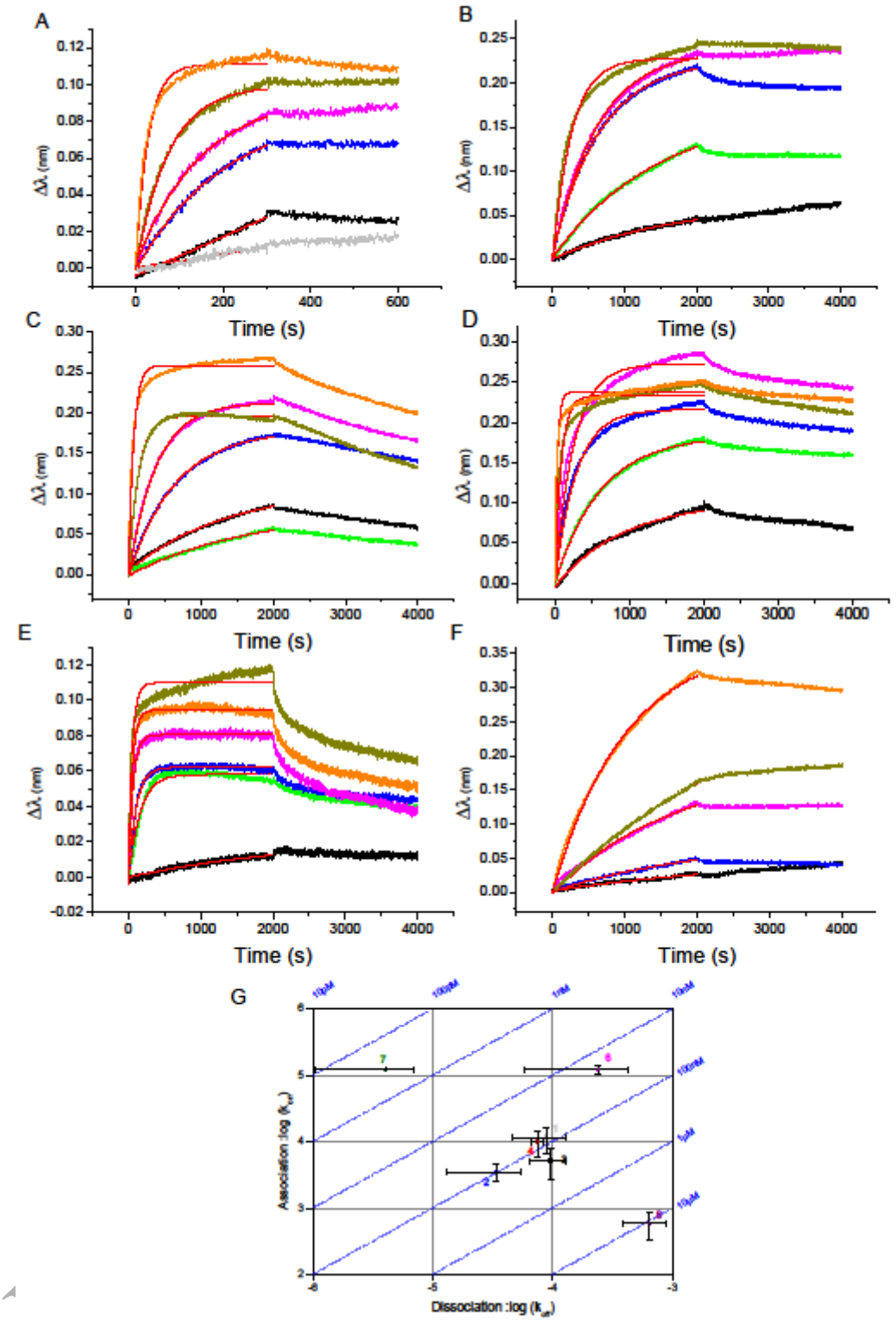

Figure 4: Sensorgrams obtained for LecB with the tetravalent and hexadecavalent glycoconjugates: A) R4oFuc **1**, B) R4tFuc **2**, C) D4oFuc **3**, D) D4tFuc **4,** E) RR16tFuc **6** and F) DD16tFuc **7**. The red lines correspond to the fitting of the association step. Each color corresponds to one ligand concentration, with the following concentrations: 35, 100, 150, 250, 350 and 1000 nM for R4oFuc **1**, 100, 250, 350,

1000 and 3000 nM for R4tFuc **2**, 100, 150, 250, 350, 1000 and 3000 nM for D4oFuc **3** and D4tFuc **4**, 10, 25, 35, 50, 75 and 100 nM for RR16tFuc **6** and 0.5, 1, 2.5, 5, 10 and 25 nM for DD16tFuc **7**. G) Two-dimensional isoaffinity kinetic plot of rate constants for the LecB–ligand interaction. The dashed blue diagonals depict the equilibrium binding constants and are shown to help with the visualization of the affinity distribution. Glycoconjugates evaluated as ligands: R4oFuc **1**, R4tFuc **2**, D4oFuc **3**, D4tFuc **4**, RR16tFuc **6**, DD16tFuc **7** and R4tMan **8**

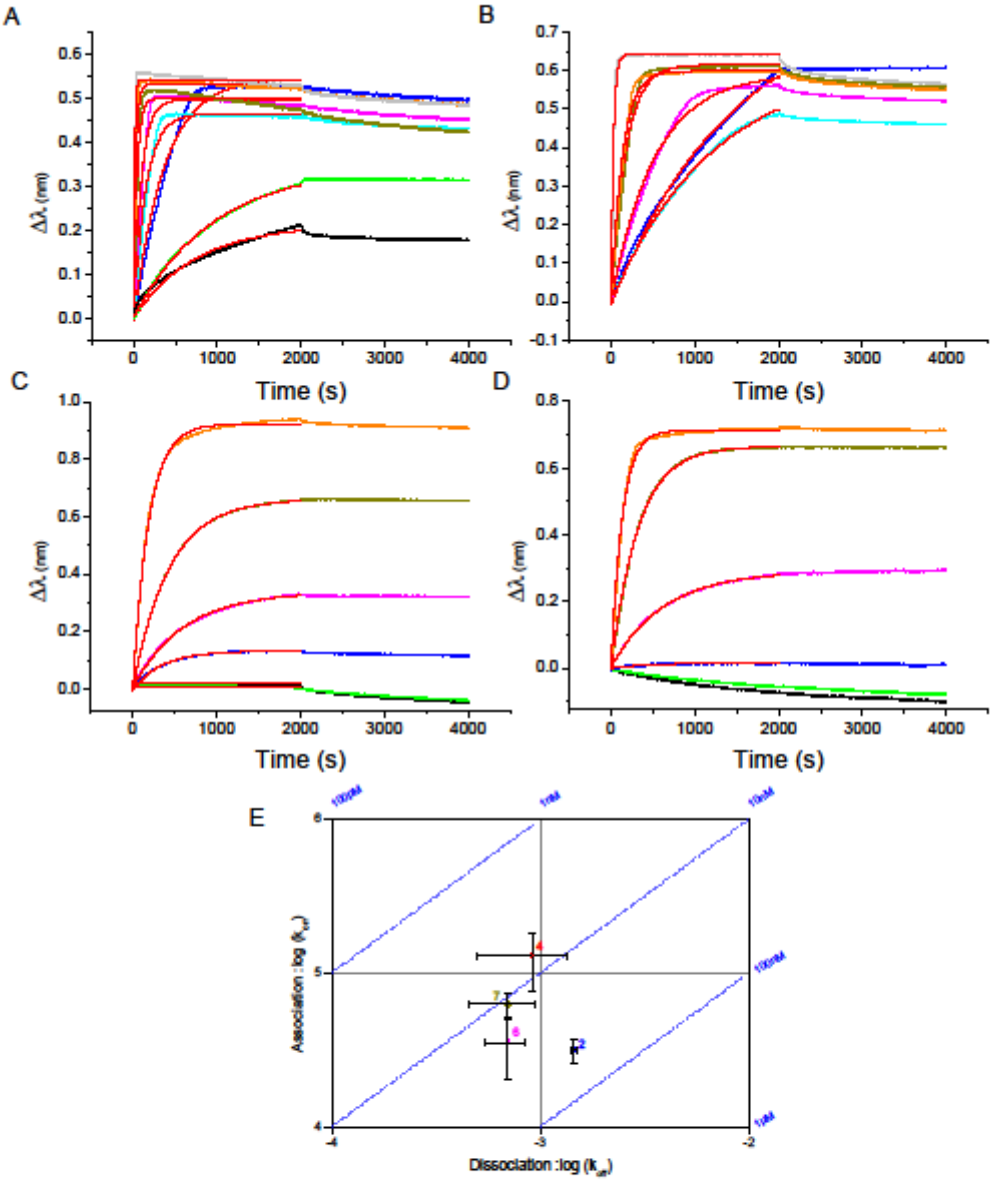

Figure 5: Sensorgrams obtained for the tetravalent (A and B) and hexadecavalent (C and D) fucose glycoconjugates with BambL: A) D4tFuc **4**, B) R4tFuc **2**, C) RR16tFuc **6**, D) DD16tFuc **7**. The red lines correspond to the fitting of the association step. The associated concentrations are 10, 25, 100, 150, 200, 350, 500 and 1000 nM for D4tFuc **4**, 100, 150, 200, 350, 500 and 1000 nM for R4tFuc **2** and 2.5, 5, 10,

25, 50 and 100 nM for RR16tFuc **6** and DD16tFuc **7**. E) Two-dimensional isoaffinity kinetic plot of rate constants for the ligand-BambL (A) interaction. The dashed blue diagonals depict the equilibrium binding constants and are shown to help with the visualization of the affinity distribution. Glycoconjugates evaluated as ligands: R4tFuc **2**, D4tFuc **4**, RR16tFuc **6**, DD16tFuc **7**

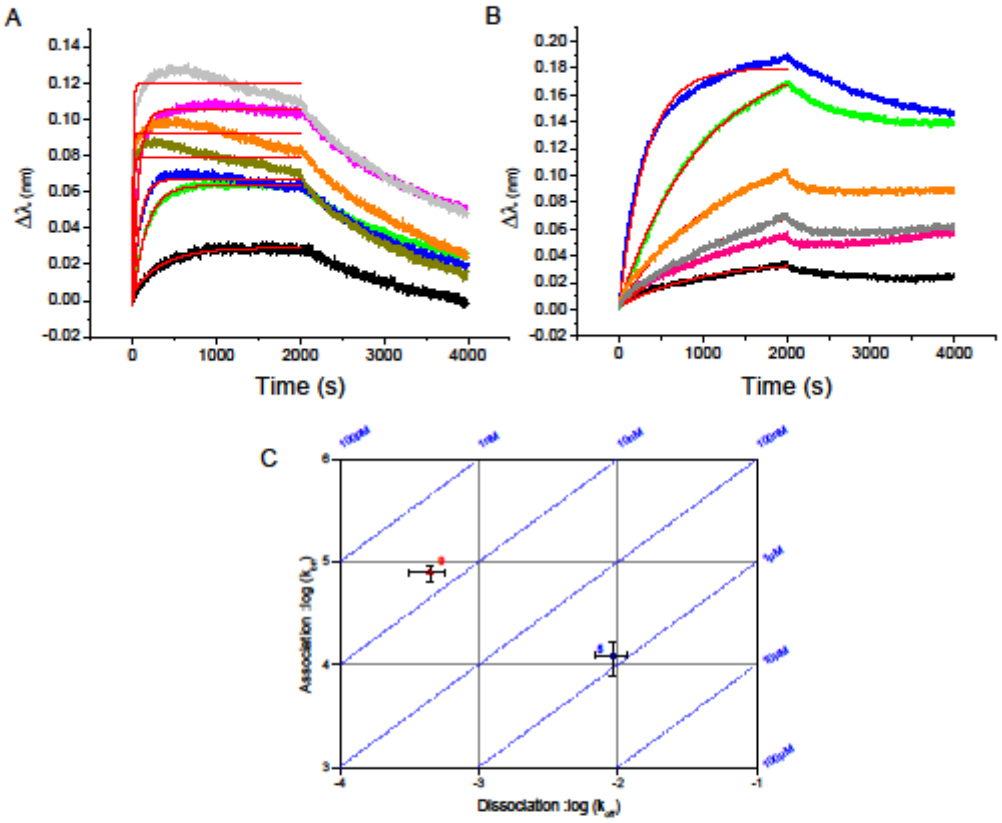

Figure 6: Sensorgrams obtained for the R4tGal **5** (A) and RR16tGal **9** (B) galactose glycoconjugates with LecA. The red lines correspond to the fitting of the association step. The associated concentrations are 0.1, 0.25, 0.5, 1, 3 and 15 µM for R4tGal **5** and 0.5, 1, 2.5, 5, 10 and 25 nm for RR16tGal **9**. C) Two-dimensional isoaffinity kinetic plot of rate constants for the ligand-LecA (B) interaction. The dashed

blue diagonals depict the equilibrium binding constants and are shown to help with the visualization of the affinity distribution. Glycoconjugates evaluated as ligands: R4tGal **5** and RR16tGal **9**

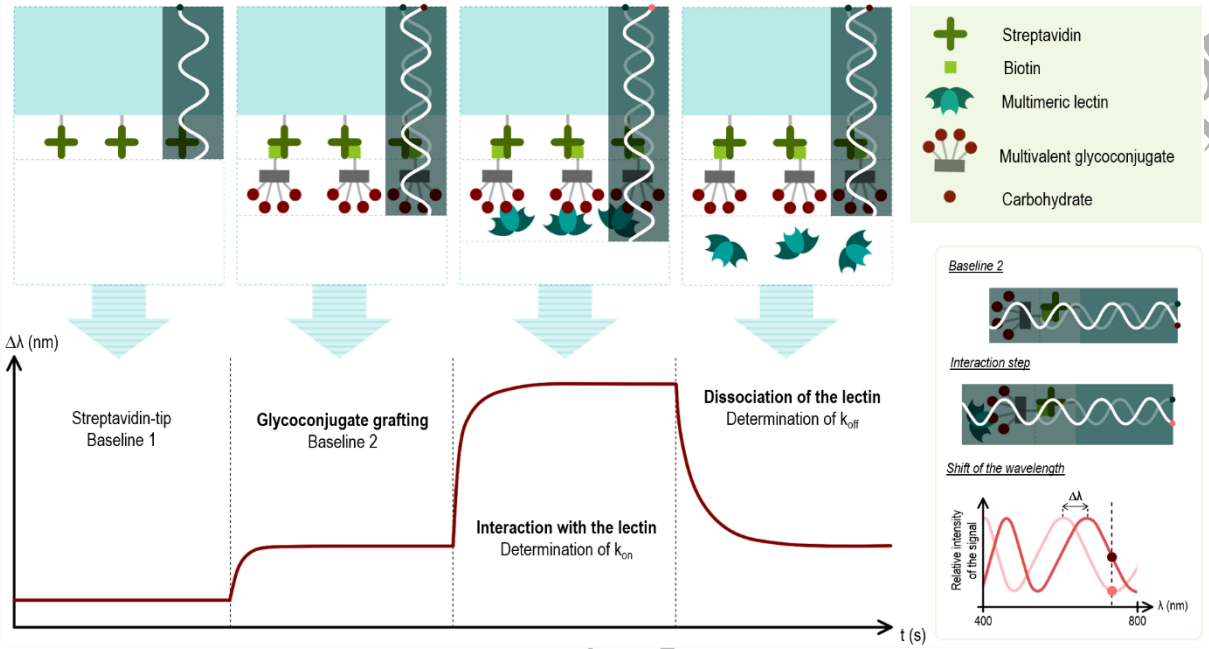

Figure 7: Schematic representation of the design used for the evaluation of the interaction between multimeric lectins (in solution) and multivalent ligands (bound to the sensor) by biolayer interferometry (BLI)

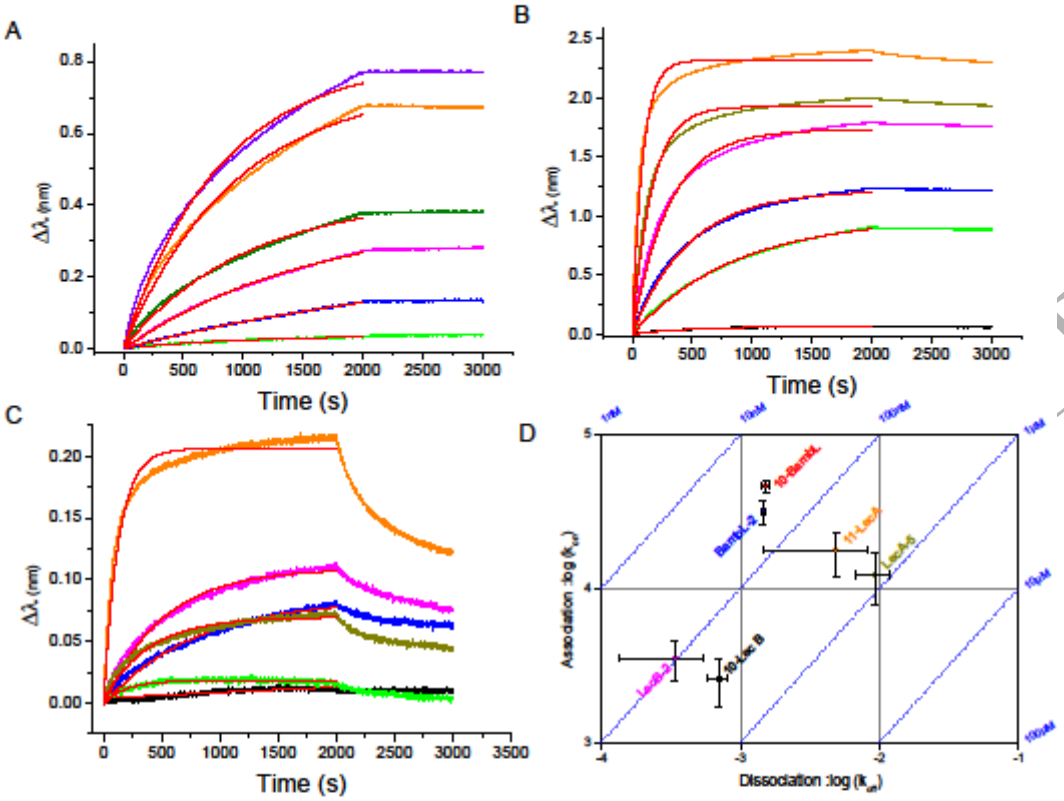

Figure 8: Sensorgrams obtained for the interaction between (A) R4tFuc-biotin **10** and LecB, (B) R4tFuc-biotin **10** and BambL and (C) R4tGal-biotin **11** and LecA. The red lines correspond to the fitting of the association step. Each color corresponds to one lectin concentration, with the following concentrations: 10, 25, 50, 100, 250 and 500 nM for LecB, 1, 10, 25, 50, 100 and 250 nM for BambL and 1, 10, 25, 50,

100 and 250 nM for LecA. D) Two-dimensional isoaffinity kinetic graph of rate constants plotted for the tetravalent ligands and the three lectins, with either the lectin or the ligand grafted on the BLI sensor. The dashed blue diagonals depict the equilibrium binding constants and are shown to help with the visualization of the affinity distribution. The complex is named X-Y with X, the molecule immobilized on the sensor and Y, the partner in solution

Tables

Molecule	K_d (nM)	k_{on} ($M^{-1}.s^{-1}$)	k_{off} (10^{-4} s^{-1})
R4oFuc **1**	76 ± 9	11600 ± 5000	8.8 ± 4.2
R4tFuc **2**	109 ± 13	3500 ± 1000	3.4 ± 2.1
D4oFuc **3**	184 ± 42	5200 ± 2500	9.6 ± 3.2
D4tFuc **4**	75 ± 11	10000 ± 4100	7.6 ± 0.8
RR16tFuc **6**	19 ± 5	123000 ± 19 400	24 ± 18
DD16tFuc **7**	0.3 ± 0.2	123000 ± 1000	0.4 ± 3

Table I: Kinetic and thermodynamic parameters of the interaction between LecB and αFuc-functionalized conjugates. The data have been obtained from Figure S 17 and Figure S 18.

Molecule	K_d (nM)	k_{on} ($M^{-1}.s^{-1}$)	k_{off} (10^{-4} s^{-1})
R4tFuc **2**	46 ± 10	31 600 ± 6 000	15 ± 7
D4tFuc **4**	7 ± 3	130 000 ± 54 100	9 ± 4
RR16tFuc **6**	20 ± 2	35 600 ± 15 200	7 ± 1.5
DD16tFuc **7**	10 ± 2	63 100 ± 12 000	7 ± 2.4

Table II: Kinetic and thermodynamic parameters of the interaction between BambL and αFuc-functionalized conjugates. The data have been extracted from Figure S 21.

Molecule	K_d (nM)	k_{on} ($M^{-1}.s^{-1}$)	k_{off} (10^{-4} s^{-1})
R4tGal **5**	750 ± 100	12 300 ± 4 500	92 ± 2.4
RR16tGal **9**	6 ± 2	79 400 ± 14 650	4.5 ± 1.3

Table III: Kinetic and thermodynamic parameters of the interaction of LecA and βGal-functionalized conjugates. The data have been extracted from the Figure S 23.

Immobilized molecule	Lectin in solution	K_d (nM)	k_{on} ($M^{-1}.s^{-1}$)	k_{off} (10^{-4} s^{-1})
R4tFuc-biot **10**	Lec B	270	2 590	7
R4tFuc-biot **10**	BambL	32	46 100	15.2
R4tGal-biot **11**	Lec A	273	17 700	48.4

Table IV: Kinetic and thermodynamic parameters obtained for the tetravalent biotinylated conjugates with the lectins in solution